Study of leakage flow in oil-free positive displacement rotary machines using particle image velocimetry

Brijeshkumar PATEL[1*], Ahmed KOVACEVIC[1], Thibaud PLANTEGENET[1], Thibault TAM[1]
[1] City University of London, London, UK, EC1V0HB
*Brijeshkumar.patel@city.ac.uk

Abstract. Rotary positive displacement machines (PDM) are widely used in industry. Oil free PDM's are used in applications where presence of oil is not allowed, but they still are not much utilised due to challenges with reliability and efficiency related to extensive thermal loads. Their efficiency is important to meet carbon footprint targets while increasing reliability will allow their wider use. The main contributor to losses is the internal leakage through clearance gaps between stationary and rotating parts driven by the differential pressure between chambers. Due to the transient nature of leakage flows in running conditions, the measurement of velocity flow field inside the clearance gap is challenging but can provide significant information about flow physics. Thus, understanding of the velocity flow field is essential for developing methods to increase efficiency without compromising reliability.

The flow field in clearance gaps can be captured using Particle Image Velocimetry (PIV) for optically accessible flows. The basic PIV system consists of a light source, camera, tracer particles, and analysis algorithms. In this study the Roots blower is used as a representative of the oil-free PDM for which the velocity field is measured inside the radial clearance gap in the running condition using the PIV technique. An extensive testing campaign has been carried out at various speeds and pressure ratios of the machine. PIV measurements were taken inside, upstream, and downstream of the clearance gap. Post-processing of PIV images allows the generation of velocity fields. These pioneering measurements of the velocity field inside the clearance in the machine operating conditions reveal interesting flow physics. Moreover, the large amount of collected experimental data provides an excellent basis for validation of simulation models and further developments.

Keywords: Positive Displacement Machines, Particle image velocimetry, Leakage flows, Velocity field, Clearance gap.

Abbreviations

Terms	Symbol
Compressed Air System	*CAS*
Field of view	*FOV*
Interrogation Windows	*IW*
Positive displacement machines	*PDM*
Particle image velocimetry	*PIV*
Pressure ratio	*PR*
Scientific complementary metal oxide semiconductor	*sCMOS*

1 Introduction

Positive Displacement Machines (PDM) work by enclosing a fluid in a trapped controlled volume before it is released at the discharge side. Nowadays, various types of PDM operating as compressors, expanders or pumps are used in many commercial applications such as

industrial, commercial of residential HVAC systems, industrial compressed air systems (CAS) and process gas systems.

Both reciprocating and rotary-type PDM include parts in relative motion. For reliability reasons, the parts in relative motion are separated by clearances and/or lubricated with oil. Two types of machines exist: oil-injected and oil-free. Oil-injected compressors use a lubricant to reduce friction and wear between parts in contact, to seal clearances between chambers and to remove heat coming from compression by direct contact of the compressed gas and oil. In oil-free compressors there is no fluid injected in the compression chamber and therefore clearances need to be provided in order to prevent contact between moving and stationary parts and to compensate for the thermal deformation of solids due to the compression process. The oil-injected compressor is a very mature technology, thus their reliability and efficiency are well-controlled and close to an optimum. Oil-free compressors still have limited use due to extensive thermal loads on elements which deform. Therefore, it is always a compromise between reliability and efficiency in oil-free compressors. Clearances play a critical role since they need to exist for reliability but lead to a significant loss of efficiency due to internal leakages between compression chambers [1], [2]. This explains the challenge in designing clearances, where a smaller clearance will produce better efficiency but reduce reliability and vice versa.

Despite the large number of reciprocating machines used especially in commercial and domestic applications, rotary machines represent a large proportion of electricity consumption, especially in industry. Saidur et al.[3] and Mousavi et al.[4] shows that CAS account for 10% of electricity consumption in the industry. When considering the International energy agency(IEA) [5] data that shows 40% of generated electricity is consumed by industry, that means around 4% of worldwide electricity is used in CAS. Similarly, based on two reports ordered by the European Commission [6] presenting the proportion of power consumption of compressors in the industry in European countries, compressors used to process gases account for approximately 1.5% of worldwide electricity consumption. The reports also showed that a larger proportion (more than 40%) of power consumption in CAS is consumed by oil-injected screw and vane compressors, while in process gas a large proportion is consumed by turbo-compressors/blowers.

In the objective of climate change mitigation, described by the latest Intergovernmental panel on climate change (IPCC) [7] report, and the net zero CO2 target adopted by governments for the next decades [8], it is essential to improve the efficiency of machines as well as reduce fossil fuel consumption. Thus, it is primordial to improve efficiency and maintain high reliability, especially for oil-free machines in order to develop their proportion in the market versus the oil-injected ones. This paper is an attempt to use Particle Image Velocimetry (PIV) to understand the physical phenomena appearing inside the oil-free machines. Specifically, to research internal clearances with an aim to counteract leakages, and consequently act on efficiency and reliability.

Internal leakage flows in PDM are mainly driven by the differential pressure between chambers, which theoretically result in a Poiseuille flow. However, the relative speed between surfaces, or surface features can affect the fluid dynamics inside the clearance [9]. So, it is necessary to understand the behaviour of these leakage flows.

It is extremely challenging to visualize flow in the clearance gap during the actual running condition of a rotating machine. Therefore, few attempts have been made over the years. Sachs [10] has developed a static experiment mimicking one (axial) plane of radial clearance in a screw compressor to visualise the flow field using the Schlieren method between the male

rotor and the casing. This extensive experiment was conducted for pressure ratios from 1.5 to 2.5, variation of gap size (from 0.1 to 0.4 mm) and surface features (roughness and shape). It is stated that the effect of moving gap boundary is very small on the flow pattern in supercritical flow conditions compared to the effect of gap shape, height, and pressure ratio. An investigation of flow through the male rotor housing clearance of screw machines was carried out by Utri [11] who compared simulation results with flow pictures obtained using the Schlieren method. It is observed for the stationary boundary, the impact of the pressure ratio and the ratio of clearance height to rotor diameter on the flow coefficient is minor. Also, the Reynolds number is found to be an important factor because it determines the thickness of the boundary layer and therefore the profile of the flow.

A numerical approach to analyse the effect of the clearances on compressor performance was developed by Kovacevic [12]. Recently, the PIV technique was investigated by Singh et al. [13] to implement during the running condition of a Roots blower but not in actual operating condition. They have observed interesting flow features such as vortexes outside the clearance. However, this study was not able to capture the flow inside the clearance. However, a series of factors deteriorating the results of the PIV test were highlighted, such as limitations in resolving flow features in regions near the gaps and the large sample size required. Numerical analyses of a Roots blower were carried out by Sun et al. [14]. It is observed that the CFD flow field agrees with experimental results in the flow pattern and velocity magnitude at certain areas but overestimates the leakage flow velocity.

However, none of these experiments were performed in the actual running condition of the machine. Therefore, this study focuses on the implementation of the PIV technique in the actual running condition of the machine to capture the leakage flow field in clearance gaps. The current study will also help to provide experimental data to validate CFD models.

2   Experimental analysis using PIV method

2.1   Optical Roots blower test rig

The Roots blower is a good representative of rotary PDM. Its straight lobes and simple shape provide an easy access for clearance visualization in operation. As shown in Figure 1(a), the Roots blower is composed of two bi-lobe rotors mounted on parallel shafts rotating in opposite direction and synchronised by a timing gear. As the fluid is trapped between the rotors and housing, it is compressed during the rotor's rotation from the inlet port to the discharge port and to the external system. In this application, the employed fluid is ambient air.

To maintain the normal operation of the blower, clearance gaps exist between rotors called the interlobe gap, between each rotor and the casing called radial tip gap and axially between the end face and the end plate called the axial gap. Precise manufacturing of these rotors enables these clearances to be very small. However, air can still pass through them. Thus, the pressure difference between discharge and suction causes air to flow back from the reservoir to the low-pressure regions through these clearances (Figure 1(b)). This flow is called internal leakage flow.
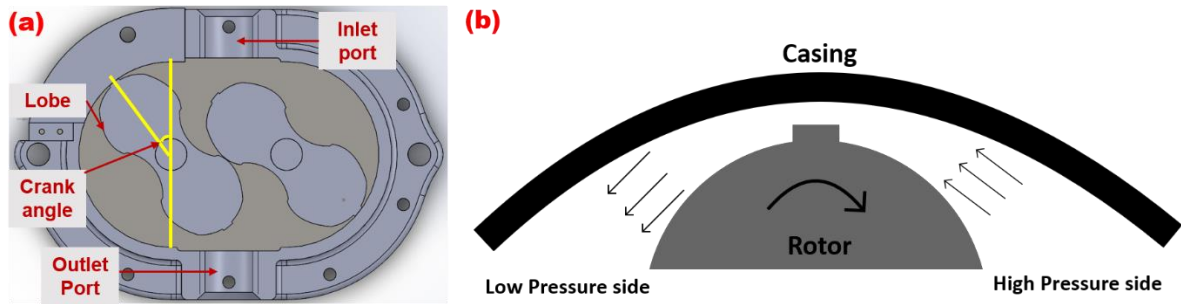
Figure 1 (a) Components of actual roots blower (b) Flow in clearance of Roots blower

This study utilises the same test rig used by Patel et al.[15] for Planar laser induced fluorescence tests, but with modifications to the suction part because the current study uses smoke as a seeding particle as shown in Figure 2. The Roots blower is connected to an electric motor by a pulley transmission system. The speed of the electric motor is regulated using a variable frequency drive (VFD). The torque meter and shaft encoders are used to measure the power and speed of the machine respectively. Pressure at the discharge side of the machine is controlled by the pressure control valve. Also, the temperature and pressure sensors are used at the suction and discharge of the machine to measure the temperature and pressure in the system. The orifice plate is used to calculated the volume and mass flow at the suction of the machine by measuring the differential pressure across the orifice plate. All sensors are connected to a National Instruments-based data acquisition system to record real time data. The basic characteristics of the Roots blower are shown in Table 1.
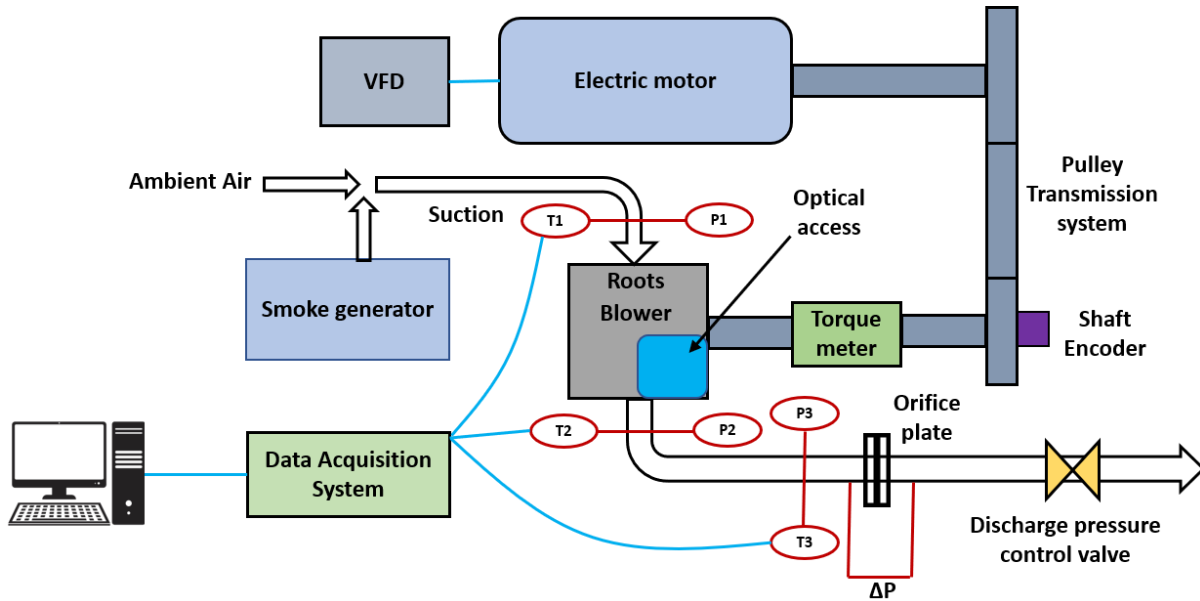

Figure 2 Schematic diagram of Roots blower test rig

Table 1 The main parameters of the Roots blower

Items	Specification	Items	Specification
Diameter of the rotor [mm]	101.3	Tip gap [mm]	0.1
Axis distance [mm]	63.12	Interlobe gap [mm]	0.17
Rotor length [mm]	50.5	Axial gap [mm]	0.15
Displacement volume [l/rev]	0.4618	Width of tip step [mm]	6.4

2.2   PIV principle and setup

Particle Image Velocimetry (PIV) is a non-intrusive optical velocity measurement technique yielding planar whole-field quantitative measurements of instantaneous and mean velocities. PIV determines a velocity field by tracking the average motion of particle groups from a pair of images that are separated by a known time delay. The technique requires the flow field to be seeded with small particles which accurately follow the flow. A dual-pulse laser is used to illuminate a thin sheet of the flow with a short time delay, Δt, between the two pulses. The light scattered by the seed particles is recorded by a double shutter camera, in this case, a camera with an sCMOS sensor, positioned normal to the laser sheet. By prescribing the time delay between pulses (Δt) and measuring the particle displacement (Δx) between the two recorded images, the velocity field is computed as $\Delta x/\Delta t$. In practice, particle displacements are computed by dividing the recorded image into sub-areas called Interrogation Windows (IW). The in-plane displacement of the particles in each IW is obtained using statistical image cross-correlation. A velocity vector map over the whole image area is obtained by repeating the cross-correlation and velocity calculation for each IW. To determine the relation between the particle image displacement in the image plane and the tracer particle displacement in the flow, a calibration is required. The displacement of the particle images between the light pulses can be determined through evaluation of PIV recordings, and for that sophisticated post-processing should be implemented. A detailed description of the PIV technique is given in [16].

Optical access to clearance gap is required for PIV, and for that purpose a part of the initial Roots blower casing was machined and replaced with an optical element made from fused silica glass. Figure 3 (a) shows the complex shape of the optical glass manufactured from the Fused silica. As shown in Figure 3 (b) & (c), optical access from both radial and axial directions of the Roots blower is provided to illuminate (radial laser access) and visualize (axial access) the flow in the radial clearance gap between the rotor tip and the housing. Due to the replacement of a part of the casing by the glass, the tip clearance gap between the lobe and the glass is increased to 0.4 mm instead of the 0.1 mm set with the rest of the casing [17].
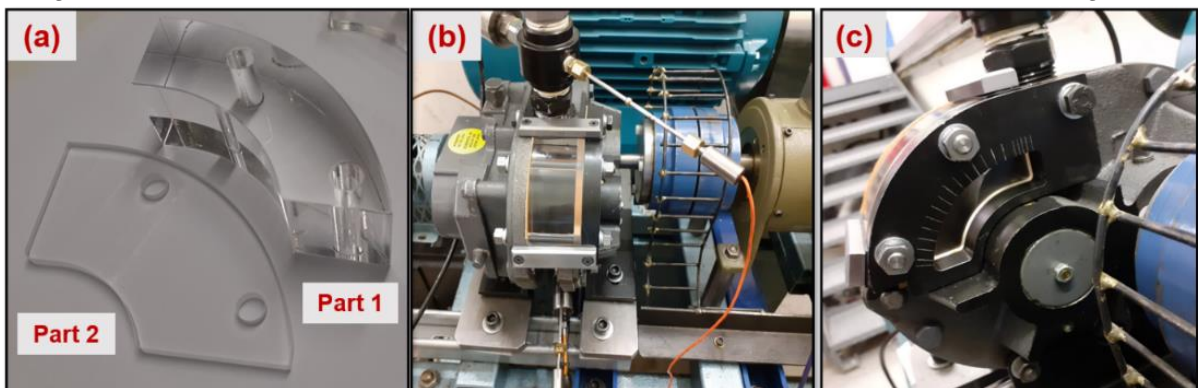

Figure 3 (a) Optical element from fused silica glass (b) Radial optical access of Roots blower (c) Optical access from the side of Roots blower[17]

A schematic of the designed PIV setup and image of actual PIV test setup is shown in Figure 4. Equipment used for the experiments are listed in Table 2.

Table 2 List of PIV equipment

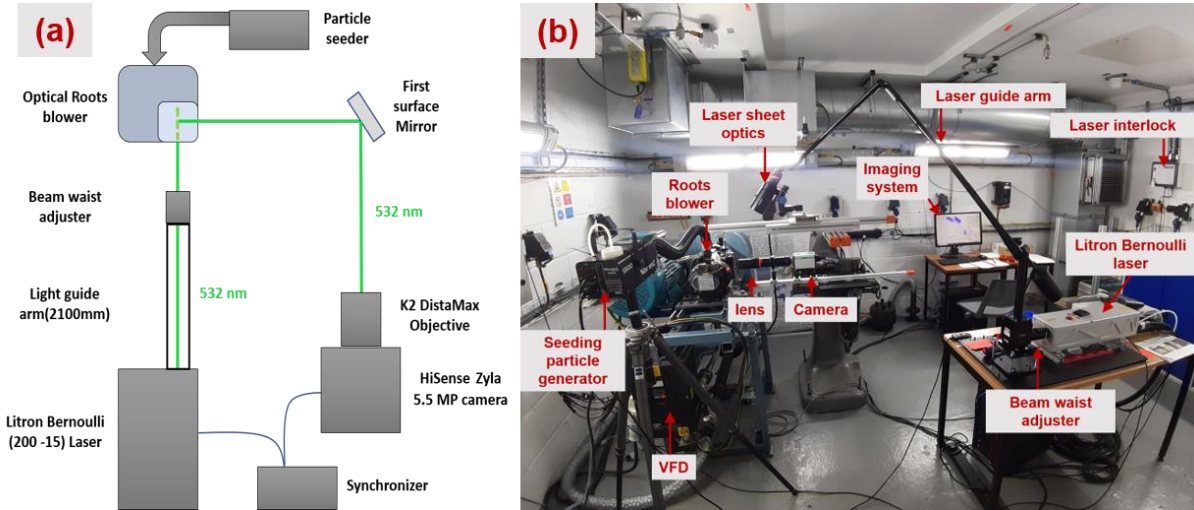| Equipment	Specification
Litron Bernoulli laser	Double pulse laser, 532nm/200mJ/15Hz
HiSense Zyla Camera	40fps, Resolution 2560 x 2160 pixels
Lens	K2 Distamax with CF2 objective
Laser guide arm	2100mm long suitable for UV& Visible light
Particle seeder	Glycol smoke generator

Figure 4 (a) PIV experiment setup layout (b) Actual PIV setup

The flow was seeded with 0.2 – 0.5 μm diameter smoke particles generated using glycol-based liquid. The flow tracking ability of the seed was validated using the particle Stokes number presented in Equation 1.

$$St = \frac{\rho_P U_F {d_P}^2}{\mu_F L_F}$$

1

where, St is the Stokes number, ρ_P is the particle density, U_F is the fluid bulk speed, d_P is the particle diameter, μ_F is the dynamic viscosity of the fluid and L_F is a characteristic length of the flow. The calculated Stokes number was lower than 1, confirming that the smoke particles closely follow the fluid streamlines.

2.3 Operating conditions and field-of-view

PIV data are captured in and around the clearance gap. As shown in the field-of-view (FOV) in Figure 5, measurements are carried out at three different locations, using CF4

objective with a K2-Distamax lens on the camera. The primary aim is to study the clearance flow. The camera was focused on the tip, at the exit of the tip and the inlet of the tip respectively. The exit of the tip is termed as the trailing edge side of the clearance which is connected with the suction chamber and the inlet of the tip is termed as the leading-edge side of the clearance which is connected with the discharge chamber are captured.
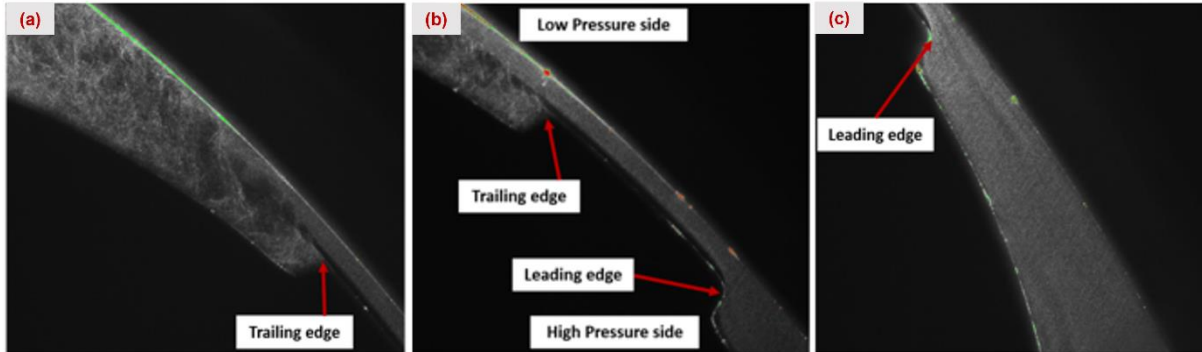

Figure 5 (a) FOV at trailing edge of clearance (b) FOV at the clearance between tip and casing (c) FOV at leading edge of clearance

Measurements at all three locations are carried out at a steady state regime with the set discharge pressure for various operating conditions, as listed in Table 3. Combinations of test conditions are created by varying machine speed from 1000 to 2000 RPM and pressure ratio from 1.2 to 1.6. All measurements are carried out at 45 degrees of crank angle and for each recording a minimum of 200 image pairs are captured.

Similarly, additional measurements are carried out in a static condition at 0 RPM. The rotor was locked at 45° angle, and measurements were performed at three pressure ratios 1.2,1.4 and 1.6 by introducing air at a higher pressure at the discharge port of the Roots blower. Current experiments have used 5 - 10 % of attenuation energy of the laser.

Table 3 Machine operating conditions

Speed (RPM)	Pressure Ratio
0	1.2
1000	1.2
1500	1.2
1800	1.2
2000	1.2
0	1.4
1500	1.4
1800	1.4
2000	1.4
0	1.6
1800	1.6
2000	1.6

2.4 PIV data processing

As per the principle of the PIV technique, it is important to work out experimental settings in the beginning, because they are a trade-off between various parameters. For that purpose, experimental conditions should be carefully set to get the desired aspect of the flow. The selection of the field-of-view (FOV) is the first step in the parameter selection. The number of

pixels on the camera chip determines the spatial resolution and the number of vectors that are obtained; in this study the sensor size is 2560 x 2160 pixels. An adaptive window sizing is applied for the cross-correlation procedure. In this method the window size will be varied from 64 x 64 pixels to 32 x 32 pixels to identify at least 8 particles in the window to calculate the vector with a 50% overlap during the cross-correlation. An established rule-of-thumb is that the particle displacements between the first and second frame should not exceed 8 pixels for the correlation. As a result, the time between the two consecutive laser pulses (dt) has been adjusted to 0.2 µs. The light sheet's width is 50 mm, and the centre portion of the light sheet is focused on the FOV which is not more than 25mm wide. Moreover, the uniformity of the light intensity is not critical because it is not an intensity based measurement such as planar laser induced florescence [18].

Cross-correlation may sometimes lead to aberrant velocity vectors. Therefore, pre-processing is performed on the images to reduce the error brought by incorrect vectors. The minimum intensity is calculated from each ensemble made up of 200 images, which is then subtracted from each individual image to remove the background noise. Pixel locking can cause measurement error measurement as well, therefore, the recorded images were evaluated to avoid pixel locking. To improve the measurement results, a coherence-filter-based post-processing is applied to the calculated raw velocity field. Dantec Dynamic Studio software was deployed in the current study for PIV data acquisition and data post-processing.

3   Experimental results

This section discusses the observations in the captured images, velocity field and other derived quantities at all three focused locations as shown in Figure 5.

Firstly, the recorded images are analysed to see the flow structure. Figure 6 shows the instantaneous raw images at various operating conditions. Seeded particles are not present near the surface of the tip, which is distinguished by the black strip across the tip. This is because of an extremely high velocity gradient at the boundary of this void region, due to the contraction of the flow and shape of the leading edge of the tip indicated by yellow circles in Figure 6. This high-velocity jet flow is entering the low pressure chamber at the trailing end of the tip creating vortexes. It is of interest to analyse the velocity vector field in these regions.
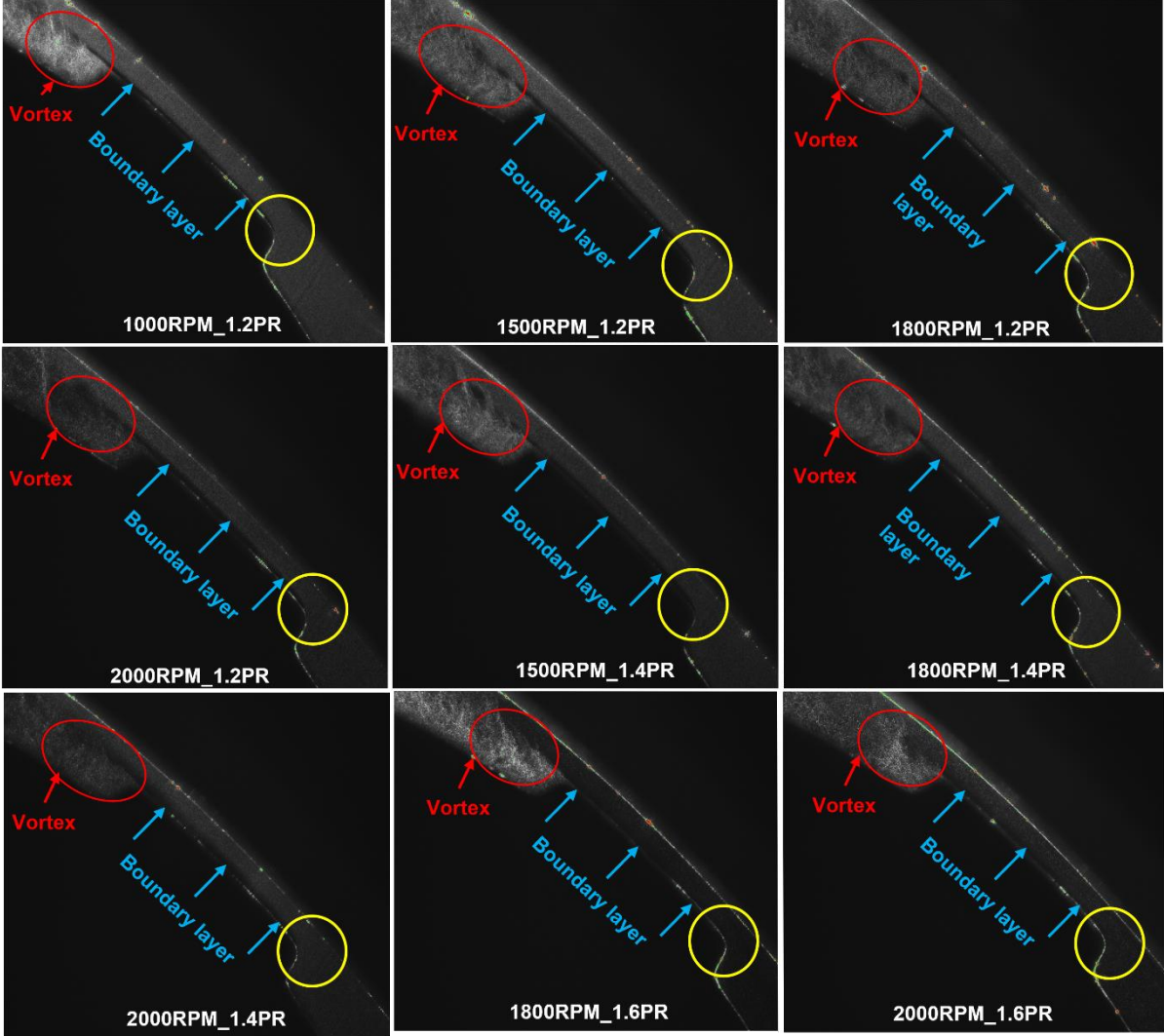
Figure 6 Raw images of flow field at various operating conditions

3.1 Velocity field in the clearance

Instantaneous velocity field is obtained for each of the 200 recorded image pairs as per the procedure described in section 2.4. The velocity field in the clearance is important to quantify the leakage flow rate, thus, it is pertinent to derive the mean velocity in the clearance, instead of extracting the instantaneous velocity field for each pair of images. However, to validate the use of mean velocity based on the average of instantaneous velocity vectors coming from several recorded images it is necessary to check the velocity fluctuation over time. Velocity fluctuation can be calculated using Reynolds' decomposition shown in equation 2.

$$u' = u - \bar{u}$$

2

where, u' is the velocity fluctuation, u is the instantaneous velocity and $\bar{u}$ is the mean velocity. The velocity fluctuation at several time steps for each operating condition has been reviewed during PIV post-processing, and an example for 1000 RPM and 1.2 PR is shown in Figure 7. As it can be seen in the Figure 7, high velocity fluctuation is observed where the seeding particles start appearing above the tip in the boundary layer. However, the velocity pattern is streamlined, and very small fluctuations are observed in the middle of the tip and near the

casing surface. This allows to derive mean velocity from the instantaneous vector fields to produce more informative vector plots.
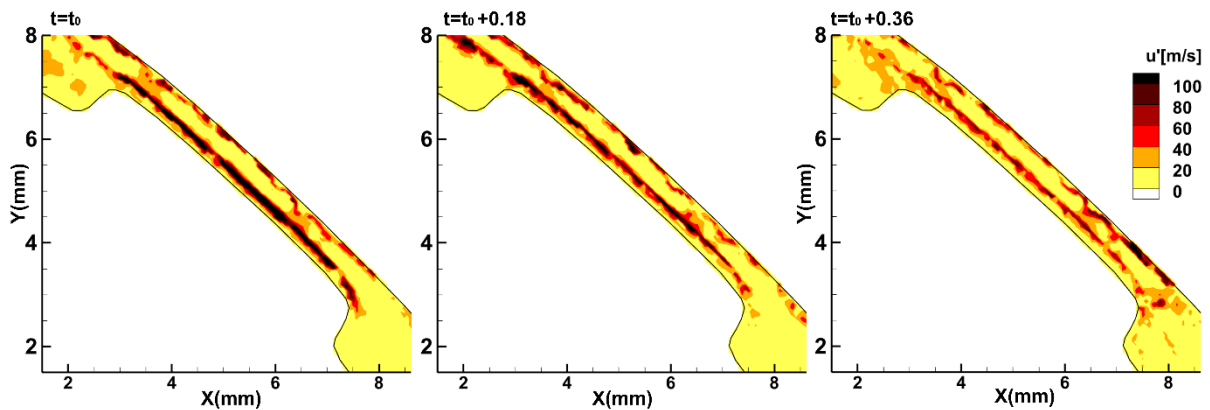

Figure 7 Velocity fluctuations in the streamwise region at reference frames: $t = t_0$, $t_0+0.18$ s, $t_0+0.36$ s for 1000RPM and 1.2PR

Mean velocity magnitude are produced using 10 instantaneous vector fields for each measurement condition, as shown in Figure 8 to Figure 10. From the magnitudes it is clearly noticeable that velocity is increasing in the clearance with the increase in pressure ratio. It is useful to perform statistical analysis to see the effect of speed and pressure difference on the velocity within the clearance. For that, velocity profiles are extracted above the centre of the clearance in streamwise direction 4mm and 5mm away from the point B over line 'C' and line 'D', respectively. The velocity near the surface of the tip is not available from PIV measurements because of the absence of the particles in this region, so extracted velocity profiles just near to the surface don't represent true values. Therefore, integral average is carried out only on the true values of the profile in the clearance.
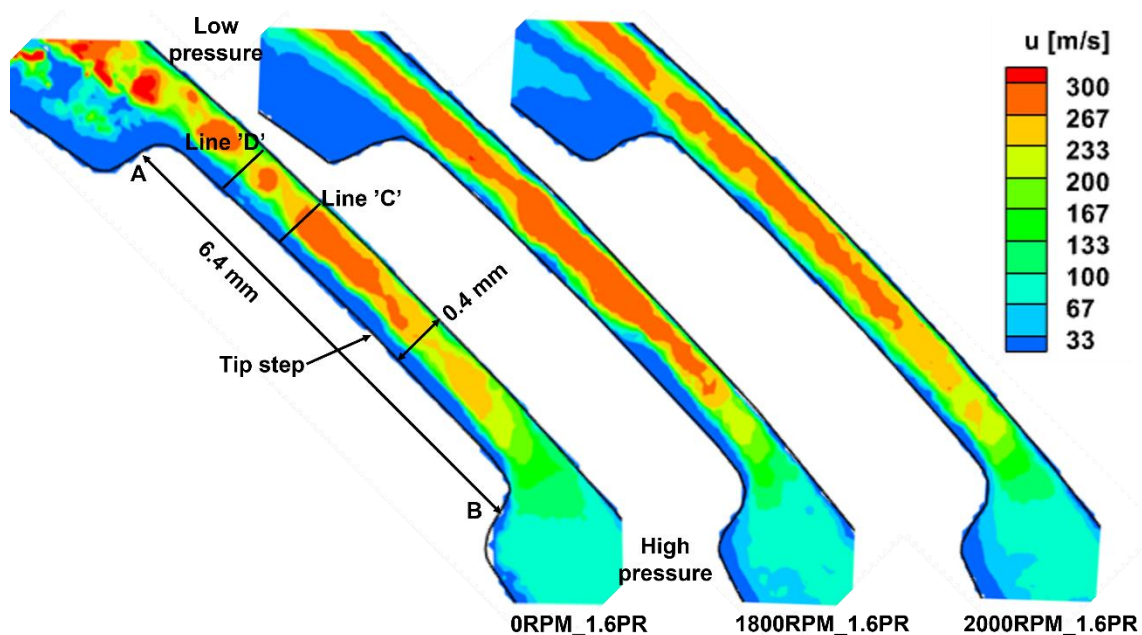

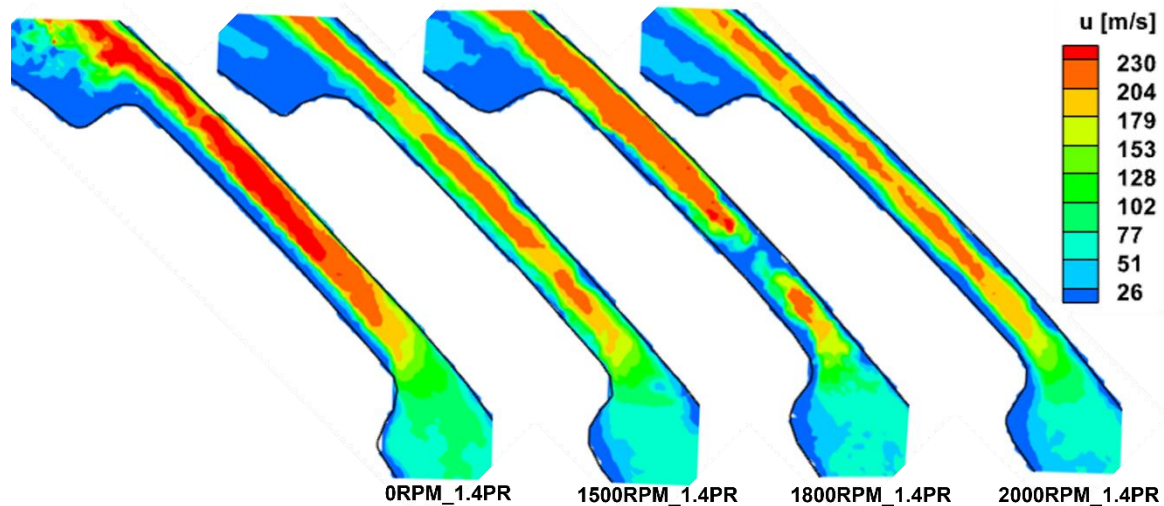**Figure 8 Mean velocity magnitudes at 1.6 PR and 0 to 2000RPM**

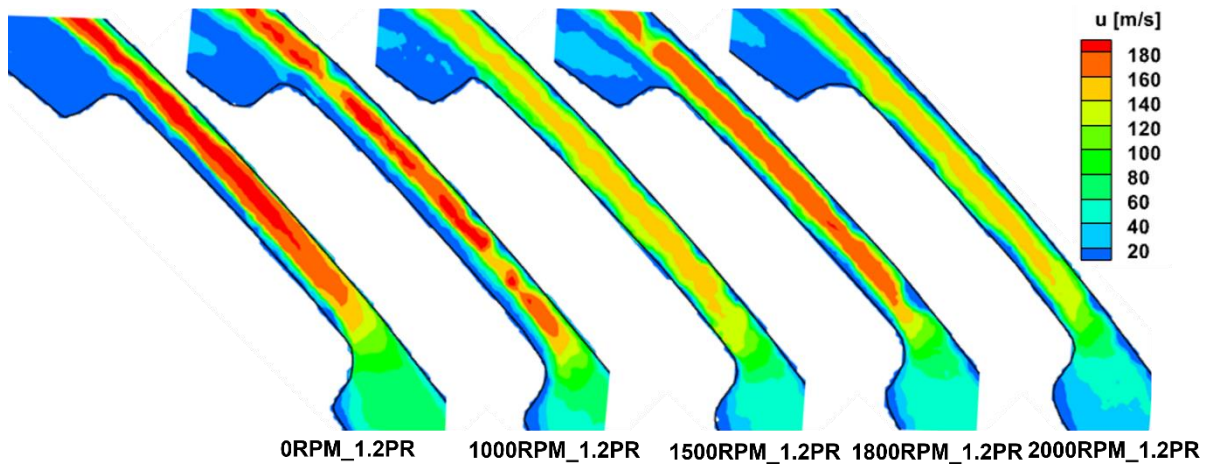**Figure 9 Mean velocity magnitudes at 1.4 PR and 0 to 2000RPM**

Figure 10 Mean velocity magnitudes at 1.2 PR and 0 to 2000RPM

Comparison of the average velocity is presented in Figure 11. It was found out that the velocity in the static condition is higher than that at all rotating conditions at the same pressure ratio. Figure 11 represents the effect of the rotational speed on the velocity inside the clearance. It seems that as rotational speed increases, the velocity of the flow in the clearance decreases. Also, with the increase in pressure ratio, the difference between velocity in static condition and rotating condition is getting smaller. Therefore, mass flow rate through the clearance at the same pressure ratio will be different between stationary and rotation conditions of the machine.
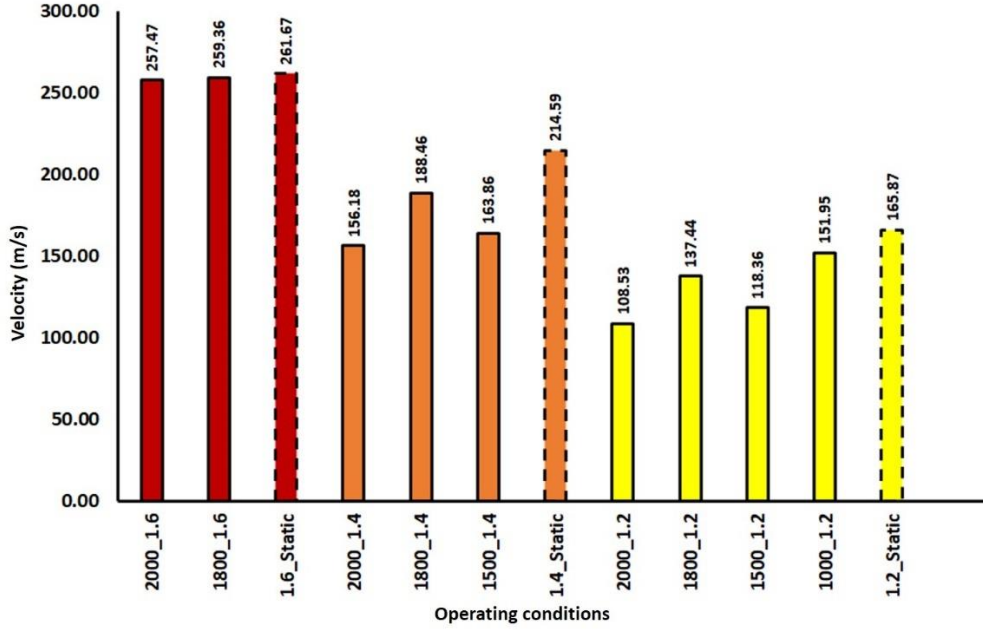
Figure 11 Comparison of average velocity in the clearance at all the measuring conditions as stated in Table 3

Average velocity profiles plotted for all running conditions are shown in Figure 12, where δ is a clearance gap length from the rotor to the casing surfaces. Maximum velocity is increasing with the increase in pressure ratio. It is interesting to note that the velocity profile in static condition of the rotor is wider than in all the running conditions. It shows a higher velocity near the casing wall in static condition and wider velocity profile when compared to the profile in the rotating condition. This confirms that the rotational speed has an effect on flow velocity inside the clearance.
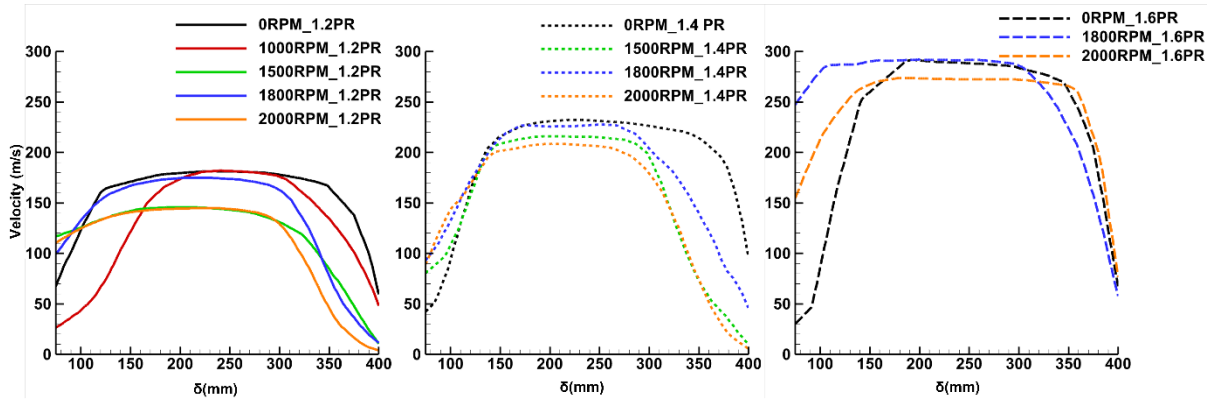

Figure 12 Velocity profile across the clearance from rotor tip to casing obtained by averaging 3 profiles considered above the center of the clearance

3.2 Flow field at the exit of the tip (trailing edge)

The high speed jet leaving the trailing edge of the tip is entering into the suction chamber. Figure 13 shows the instantaneous velocity vectors at $t = t_0$, $t_0+0.09$ s and $t_0+0.18$ s, superimposed on the vorticity contour at 2000 RPM and 1.2,1.4 &1.6 PR. Vorticity is derived from the measured planar data. Planar data gradients in the z-direction cannot be calculated. Therefore, only the rotation around the z-axis can be determined using equation 3,

$$\omega_z = \frac{\partial V}{\partial x} - \frac{\partial U}{\partial y}$$
3

where, ω_z is the rotation around z axis, x is the direction in x axis, y is the direction in y axis, V is the velocity component in y direction, U is the velocity component in x direction. In the trailing region of the tip, a noticeable level of vorticity is observed along with vortex rings. In this region, separation of the flow is taking place at the exit of the tip clearance, because of that vortices are generated, and they are travelling downstream of the flow. The shedding pattern from the trailing edge is complex, and the high frequency fluctuation is observed due to the unsteadiness of the flow. It is clearly visible that the flow field is highly dynamic when the flow exits from the trailing edge of the tip. The vortices are created by two layers of air which are close to one another but are moving in opposite directions and at different speeds. This phenomenon is similar to the Kelvin-Helmholtz instability [19]. The Kelvin–Helmholtz instability is a fluid instability that occurs due to the velocity shear in a single continuous fluid or a velocity difference across the interface between two fluids. Vorticity contours in Figure 13 indicate that it is getting stronger with an increase in pressure ratio. Additionally, the vortex is evolving and increasing as it moves away from the tip edge, which indicates the rolling-up process of the vortex rings. Vortices are responsible for mixing of the leaked gas and the gas existing in the chamber. However, as it is depicted in Figure 14, vortices in the stationary condition at the same pressure ratios are absent, which clearly shows the impact of rotor rotation on vortex generation. During running conditions of the machine, the rotor drags the fluid along its surface which interacts with the high-velocity leakage coming out of the trailing edge of the tip and creates a highly dynamic vortex field.

Swirl strength is also derived from the velocity vector field to see the behaviour in vortices, as shown in Figure 15. Swirl strength represents the strength of the secondary flows. The interesting nature of successive negative and positive swirl strengths is observed. The intensity of swirl strength decreases as flow moves away from the trailing edge during running conditions. However, the intensity remains strong even far from the trailing edge in static measurements, which is witnessed by the sharp long strip of swirl strength contour observable in static conditions. Also, swirl strength seems to be increasing with the pressure ratio.
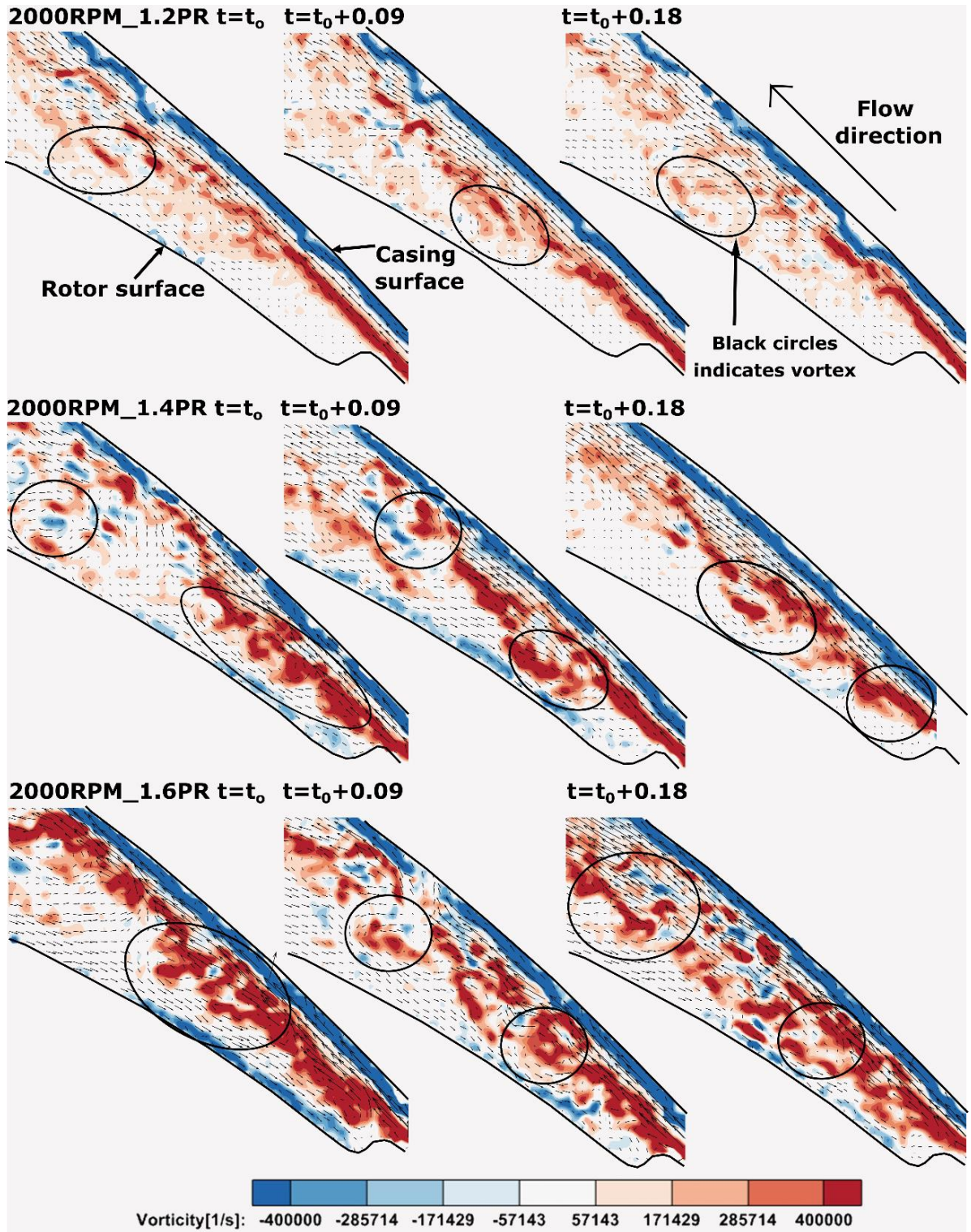
Figure 13 Instantaneous vorticity contours: $t = t_0, t_0+0.09$ s, $t_0+0.18$ s **at 2000 RPM and 1.2, 1.4 & 1.6 PR superimposed with velocity vectors**
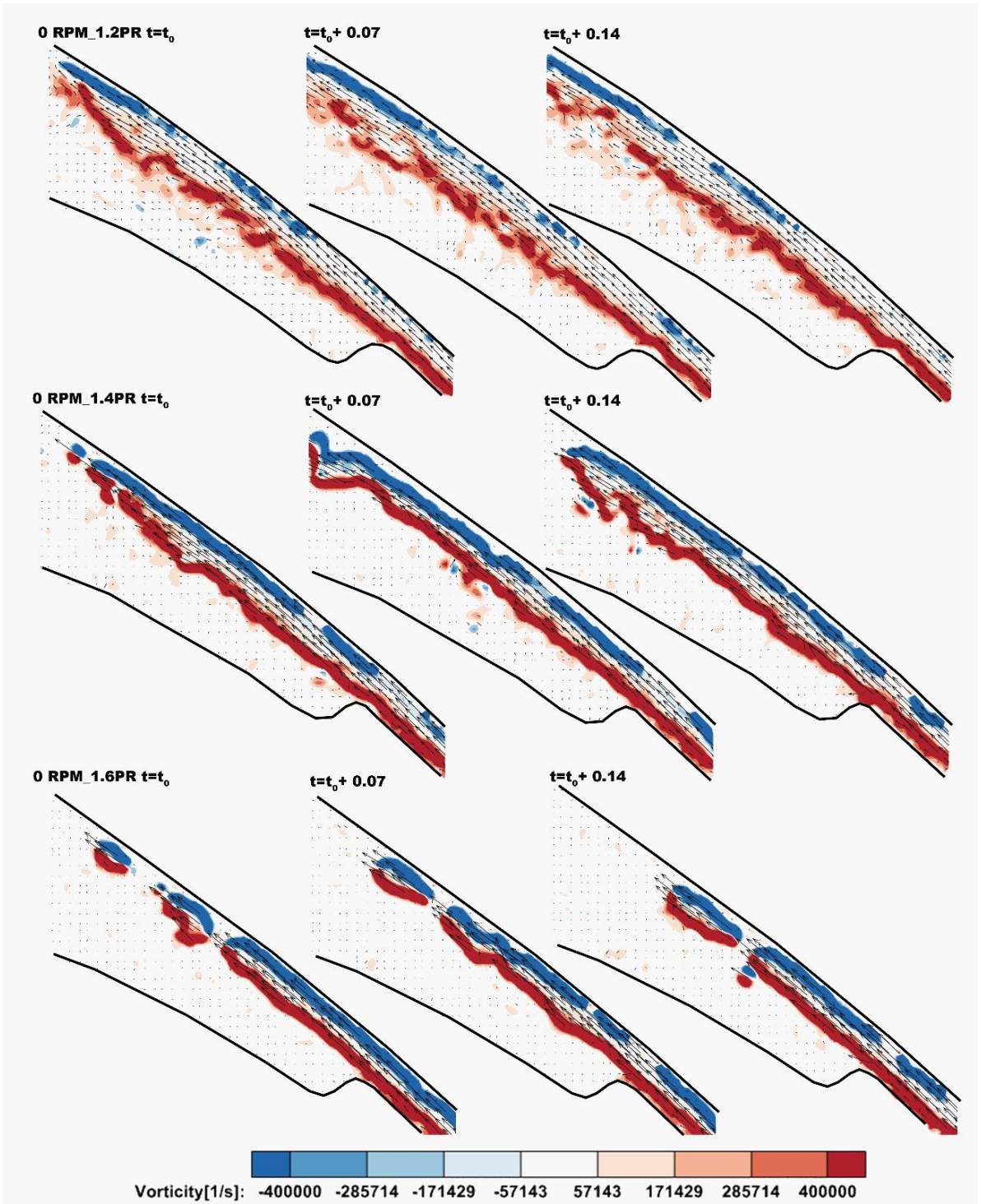
Figure 14 Instantaneous vorticity contours: $t = t_0$, $t_0+0.07$ s, $t_0+0.14$ s **at 0 RPM and 1.2, 1.4 & 1.6 PR superimposed with velocity vectors**
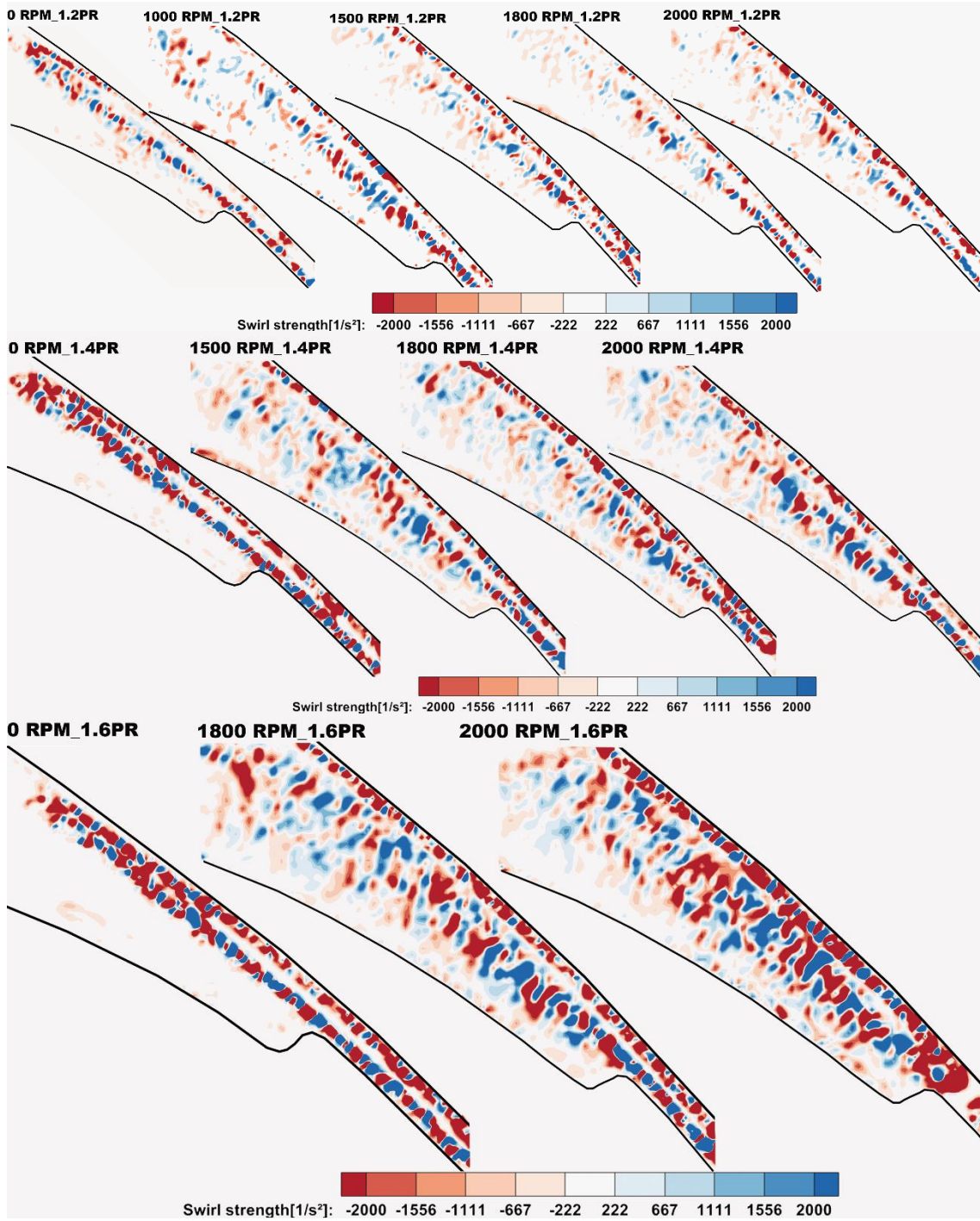
Figure 15 Swirl strength at all the measured condition at trailing edge of the tip (contours are derived from the average of 10 instantaneous plots)

3.3   Measurement at the entrance of the tip

Velocity measurements are also carried out for the flow field at the entrance of the tip. Shear in the fluid flow can be derived from velocity gradient, and it is directly proportional to the velocity gradient. To provide further insight into the flow structure, the velocity gradient in the x-y plane is calculated using equation 4 as a gradient in the z-direction cannot be calculated for planar data.

$$\tau_{xy} = \frac{\partial V}{\partial x} + \frac{\partial U}{\partial y} \qquad\qquad 4$$

where, τ_{xy} is a velocity gradient in the x-y direction. Figure 16 shows the result as a shear stress gradient contour derived from the velocity vector field. It is observed that regions of high shear stress gradient are concentrated around the surface of the lobe. Shear stress grows as flow moves further towards the leading edge of the tip, distinguished by the thick shear stress layer depicted at the base of the tip. While on the casing surface negative shear stress is observed in all cases. These extreme positive values show that the flow attaches to the rotor surface more than it does to the casing surface.
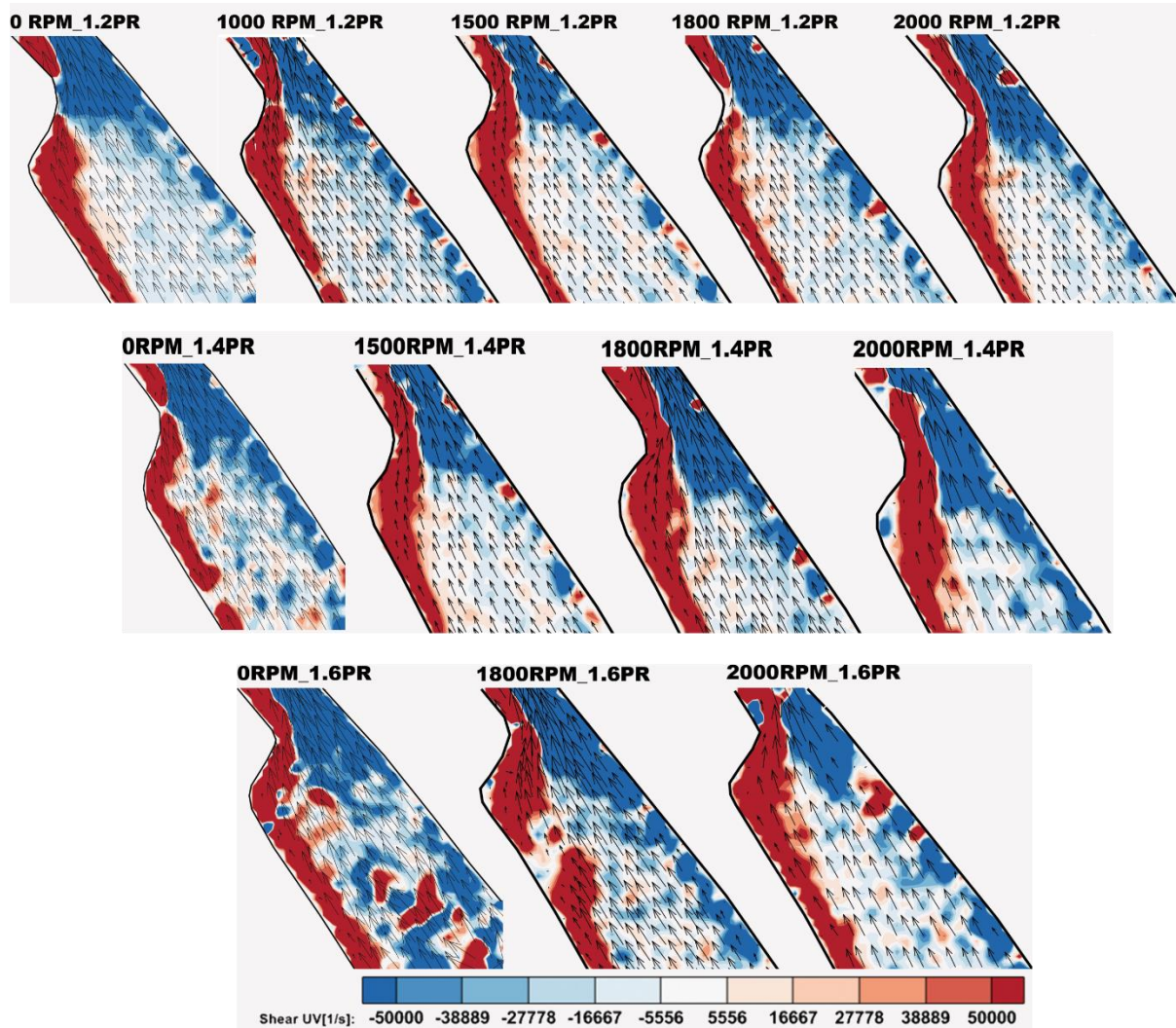

Figure 16 Contour of shear stress for all the operating conditions over the average flow field of 10 instantaneous vector field superimposed with velocity vectors

The velocity fluctuation in the region of the leading edge is calculated using Reynolds decomposition (Equation 2). Instantaneous velocity fluctuations at three different speeds and pressures are presented in Figure 17. The high local velocity fluctuations observed in this area and its fluctuation increases with increased pressure ratio. It is because air is experiencing compression from the large chamber to the smaller clearance gap.
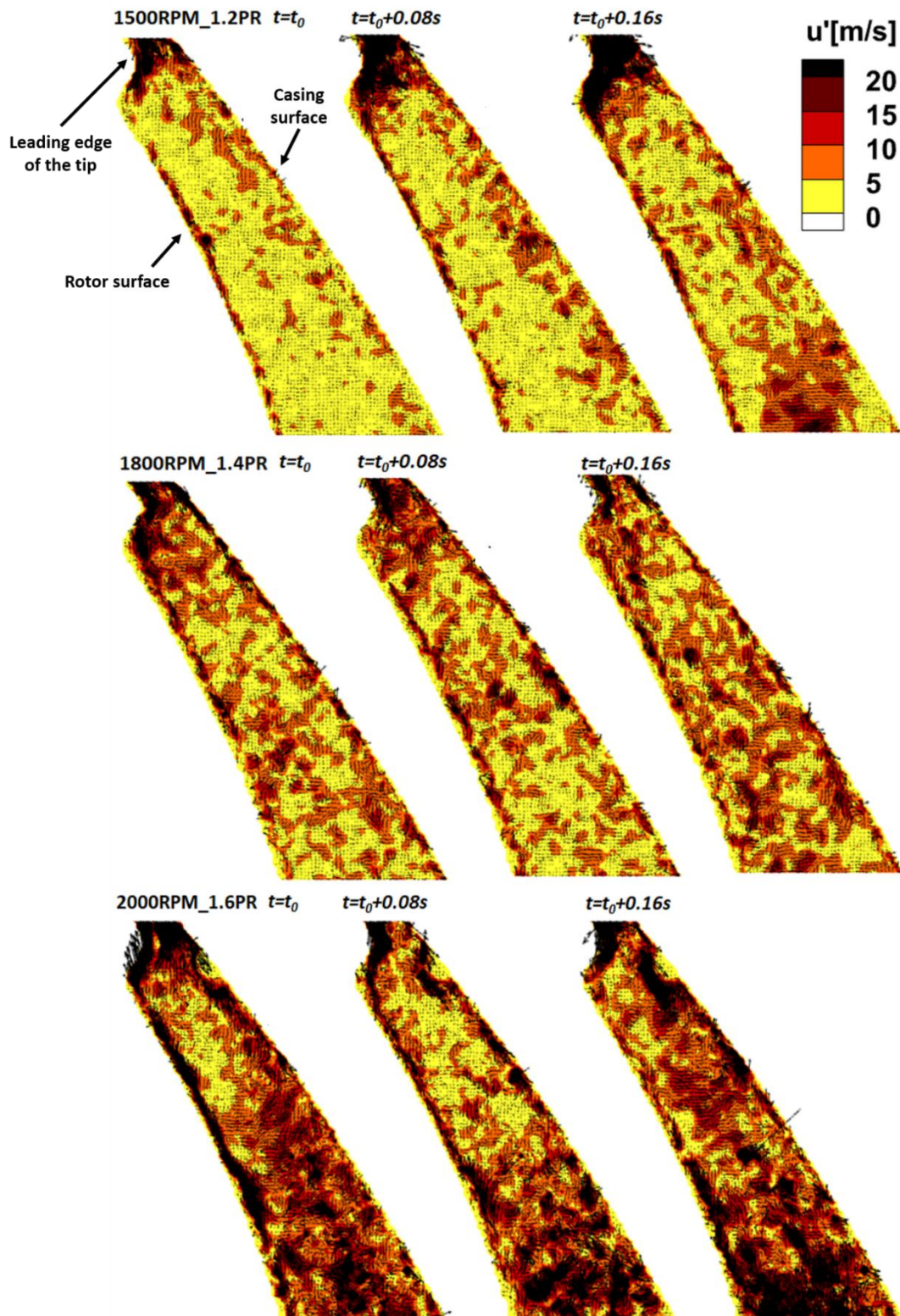
Figure 17 Velocity fluctuations at 1500RPM_1.2PR, 1800RPM_1.4PR and 2000RPM_1.6PR

4   Conclusion

This study examines the characteristics of leakage flows in rotary positive displacement machines in actual running conditions and uses a Roots blower for the analysis. An optical method was successfully applied to investigate the flow field of leakage flows. Specifically,

PIV flow visualization was used to obtain the flow field structure of the leakage flow at various speeds and pressure ratios.

The statistical analysis of the flow through the clearance gap indicates the clear influence of rotational speed on the average velocity of the flow, and hence also on the leakage flow rate through the clearance gap. The average velocities in static conditions were found to be higher than all the velocities measured in running conditions. The magnitude of velocity near the casing wall was also found to be higher in static conditions than in running conditions.

The flow field was captured inside the clearance gap, at the exit of the tip and at the entrance of the tip. PIV measurements confirmed the presence of secondary flows in the leakage flow region. When flow enters the clearance gap from the high-pressure chamber, a higher shear stress gradient was observed on the rotor surface when compared to the casing surface. Flow velocity increased drastically upon it's entry into the clearance gap. At the entrance of the tip, flow separation was observed due to the very high flow velocity and a boundary layer was formed over the entire span of the tip without any reattachment. Flow exited from the trailing edge of the tip as a jet. Vortex structure similar to 'Kelvin-Helmholtz Instability' are present, which grew in size as it moved away from the trailing edge. In summary, Figure 18 represents typical flow structures observed in the leakage flows of the Roots blower using PIV measurements. Namely, it depicts the boundary layer over the tip, vortices at the exit of the tip, the high shear gradient over the surface of the lobe on the high-pressure side, and velocity fluctuations in the high-pressure chamber near the entrance to the clearance gap. The conclusions drawn here can be applied to other types of rotary positive displacement machines such as screw compressors, screw expanders, and vane compressors where pressure difference between internal chambers is in the range of the experiments presented here. Also, the proposed experimental method can be adapted to assess leakages when the working fluid is mixed with lubrication oil. In this case, the major challenge would be the selection of suitable seeding particles because seeding particles should be compatible with working fluid and lubricant.
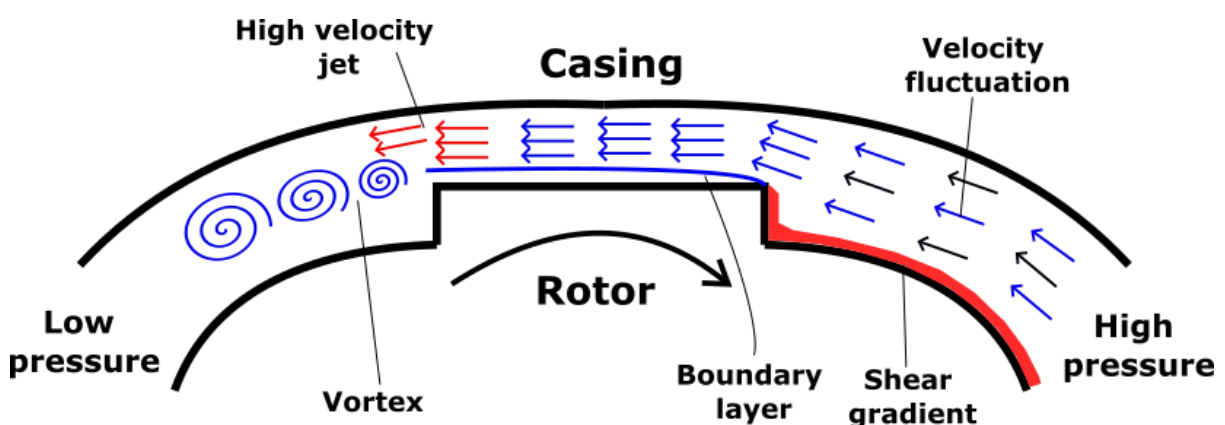

Figure 18 Schematic of flow structures found from the measurement in leakage flows

Moreover, this extensive set of experimental results provides a good basis to validate CFD leakage flow models. The observed flow field also suggests that leakage flow rate can be reduced by applying a specific tip geometry to disrupt the boundary layer. Therefore, future experiments will repeat flow field measurements in running condition with varying tip shapes to verify this hypothesis.

5 Acknowledgement

6 Declaration of Interests

The authors report no conflict of interest.

7 References

[1]   J. S. Fleming and Y. Tang, "The analysis of leakage in a twin screw compressor and its application to performance improvement," *Proc. Inst. Mech. Eng. Part E J. Process Mech. Eng.*, vol. 209, no. 2, pp. 125–136, 1995, doi: 10.1243/PIME_PROC_1995_209_239_02.

[2]   A. M. Joshi, D. I. Blekhman, J. D. Felske, J. A. Lordi, and J. C. Mollendorf, "Clearance analysis and leakage flow CFD model of a two-lobe multi-recompression heater," *Int. J. Rotating Mach.*, vol. 2006, pp. 1–10, 2006, doi: 10.1155/IJRM/2006/79084.

[3]   R. Saidur, N. A. Rahim, and M. Hasanuzzaman, "A review on compressed-air energy use and energy savings," *Renew. Sustain. Energy Rev.*, vol. 14, no. 4, pp. 1135–1153, 2010, doi: 10.1016/j.rser.2009.11.013.

[4]   S. Mousavi, S. Kara, and B. Kornfeld, "Energy efficiency of compressed air systems," *Procedia CIRP*, vol. 15, pp. 313–318, 2014, doi: 10.1016/j.procir.2014.06.026.

[5]   "IEA - International Energy Agency." https://www.iea.org/fuels-and-technologies/electricity

[6]   V. Holsteijn En Kemna, M. Van Elburg, and R. Van Den Boorn, "Preparatory study on Low pressure & Oil-free Compressor Packages," no. June, p. 289, 2017, [Online]. Available: www.eco-compressors.eu

[7]   Intergovernmental Panel on Climate Change, "Climate Change 2022 - Mitigation of Climate Change - Full report," 2022.

[8]   U. C. C. United Nations Climate Change Conference, "the Glasgow," *Cop26 Glas. Clim. Pact*, p. 28, 2021.

[9]   M. Kadivar, D. Tormey, and G. McGranaghan, "A review on turbulent flow over rough surfaces: Fundamentals and theories," *Int. J. Thermofluids*, vol. 10, p. 100077, 2021, doi: 10.1016/j.ijft.2021.100077.

[10]   R. Sachs, "Experimental investigation of Gas flows in screw machines," University of Dortmund, 2002.

[11]   M. Utri, S. Höckenkamp, and A. Brümmer, "Fluid flow through male rotor housing clearances of dry running screw machines using dimensionless numbers," *IOP Conf. Ser. Mater. Sci. Eng.*, vol. 425, p. 012033, Nov. 2018, doi: 10.1088/1757-899x/425/1/012033.

[12]   A. Kovacevic, N. Stosic, and I. K. Smith, *Screw Compressors- Three Dimensional Computational Fluid Dynamics and Solid Fluid Interaction*, vol. 53, no. 9. 2008. doi: 10.1017/CBO9781107415324.004.

[13]   G. Singh, S. Sun, A. Kovacevic, Q. Li, and C. Bruecker, "Transient flow analysis in a Roots blower: Experimental and numerical investigations," *Mech. Syst. Signal Process.*, vol. 134, p. 106305, 2019, doi: 10.1016/j.ymssp.2019.106305.

[14]   S. Sun, G. Singh, A. Kovacevic, and C. Bruecker, "Experimental and Numerical Investigation of Tip Leakage Flows in a Roots Blower," *Designs*, vol. 4, no. 1, p. 3, 2020, doi: 10.3390/designs4010003.

[15]   B. Patel, A. Kovacevic, A. Charogiannis, M. N. Alam, and M. Schütte, "The use of laser-induced fluorescence to measure temperature in the leakage gaps of oil-free positive displacement rotary machines," *Meas. J. Int. Meas. Confed.*, vol. 185, no. August, p. 110057, 2021, doi: 10.1016/j.measurement.2021.110057.

[16] M. Raffel, C. Willert, S. Wereley, and J. Kompemhans, *Particle Image Velocimetry*, Second \ed. Springer,New york.

[17] B. Patel, A. Kovačević, and A. Krupa, "On Measuring Velocity and Temperature in Leakage Flows of Oil Free Rotary Positive Displacement Machines," in *New Technologies, Development and Application IV*, 2021, pp. 763–773. doi: https://doi.org/10.1007/978-3-030-75275-0_84.

[18] B. Patel, A. Kovacevic, A. Charogiannis, and Md nahinul Alam, "Development of State-of-the-art Experimental Technique to Investigate Temperature Field in Leakage Flows of Positive Displacement Machines," in *International Compressor Engineering Conference, Purdue University*, 2021.

[19] B. Cushman-Roisin, "Kelvin - Helmholtz instability as a boundary-value problem," *Environ. Fluid Mech.*, vol. 5, no. 6, pp. 507–525, 2005, doi: 10.1007/s10652-005-2234-0.